Valorization of Polluted Biomass Waste for Manufacturing Sustainable Cathode Materials for the Production of Hydrogen Peroxide

Álvaro Ramírez , Martin Muñoz-Morales ,
Francisco Jesús Fernández-Morales , Javier Llanos

PII: S0013-4686(23)00561-3
DOI: https://doi.org/10.1016/j.electacta.2023.142383
Reference: EA 142383

To appear in: *Electrochimica Acta*

Received date: 14 December 2022
Revised date: 27 February 2023
Accepted date: 9 April 2023

Please cite this article as: Álvaro Ramírez , Martin Muñoz-Morales , Francisco Jesús Fernández-Morales , Javier Llanos , Valorization of Polluted Biomass Waste for Manufacturing Sustainable Cathode Materials for the Production of Hydrogen Peroxide, *Electrochimica Acta* (2023), doi: https://doi.org/10.1016/j.electacta.2023.142383

Highlights

- High metal content phytoremediation waste was valorized for the production of H_2O_2
- Hydrothermal carbonization+activation is a suitable technique for valorization
- Hydrochar activated by KOH (HC-KOH) showed the best electrochemical behavior
- H_2O_2 accumulation with HC-KOH was close to 70% that of Vulcan XC72 (CB)
- HC-KOH and HC1000 (activated at 1000°C) enhance (40%) the production of OH· *vs* CB

Valorization of Polluted Biomass Waste for Manufacturing Sustainable Cathode Materials for the Production of Hydrogen Peroxide

Álvaro Ramírez, Martin Muñoz-Morales, Francisco Jesús Fernández-Morales, Javier Llanos*

Department of Chemical Engineering, Faculty of Chemical Sciences & Technologies, Ciudad Real, Universidad de Castilla-La Mancha, Ciudad Real 13071, Spain

***Corresponding author**: javier.llanos@uclm.es

Abstract

A circular economy approach was followed to convert biomass wastes polluted with metals (obtained from phytoremediation processes) to generate electroactive carbon materials to be used in the electrochemical production of hydrogen peroxide. Carbon materials were pretreated using hydrothermal carbonization at 200ºC and 130 g soil mL^{-1} water and post treated through pyrolysis at different temperatures (300ºC, 500ºC and 1000ºC) and using different chemical precursors as KOH or H_3PO_4. These materials would modify the carbon paper (CP) cathodes to substitute the commonly used carbon black (CB), that comes from fossil fuels. Porosity, thermochemical behavior, electrical conductivity, electrocatalytic response and H_2O_2 accumulation tests were evaluated to determine the potential performance of these materials in the electrochemical production of hydrogen peroxide. Delays in mass losses observed in thermogravimetric studies indicate the improvement of the thermal stability of materials which are related with the highest electrical conductivity (that correspond to hydrochar pyrolyzed at 1000

ºC). High specific surface areas (1097 and 704 m^2/g) were also found with hydrochars treated with chemical precursors with values even superior to commercial CB. Results show that all activated hydrochars present electrocatalytic activity towards the production of hydrogen peroxide and that the materials chemically activated with KOH can achieve a 70% of the H_2O_2 production obtained with commercial CB. Moreover, it was found that the presence of metals in the synthesized materials may promote a Fenton-like reaction, increasing by 40% the generation of hydroxyl radicals with respect to commercial CB. This paramount finding opens the window for the use of this phytoremediation waste to produce sustainable electrode materials for upgraded electrochemical advanced oxidation processes.

Keywords: Hydrochars; Valorization, Hydrogen peroxide, Activation treatments, Hydroxyl radicals

1. Introduction

Metal extraction activities are a clear example of productive processes that have polluted natural resources for centuries. Currently, the management of waste generated as a result of mining activities in Europe is covered by European Directive 2006/21/EC on the management of waste from extractive industries. However, the mining activities carried out previously (most of them in countries as Spain) have often been abandoned, generating a severe pollution problem. Thus, there are numerous international studies that show how intensive mining activities have produced a large amount of waste rich in metals such as Pb, Zn, Cu, As, Hg or Cd in water and soil surrounding abandoned mining activities, which has a direct impact on the use of these resources and poses a risk to public health [1, 2].

In this regard, phytoremediation technologies for environmental remediation, which are based on the utilization of plants (aquatic macrophytes used in constructed wetlands for wastewater treatment, or terrestrial plant species for the treatment of sludge and polluted soils), are extensively used worldwide and they are usually the focus on new research works and projects in order to improve and optimize their performance. Plants used in such technologies capture, metabolize and/or accumulate different types of pollutants, and they strongly contribute to environmental remediation involved in a complex system of physical, chemical and biological mechanisms [3].

In the specific case of the use of phytoremediation processes for the treatment of mining waste, plants can hardly metabolize metals, so they basically accumulate them in their structure, which results in the accumulation of large quantities of metals in the biomass generated in this type of treatment [4, 5]. This accumulation does not only occur in plant-based treatment systems, but also in plants growing naturally in contaminated mining environments [6]. This accumulation represents an environmental issue that hinders the application of these treatment technologies, and that can lead to the introduction into the food chain of pollutants that are not metabolized by plants.

From the point of view of integral management and valorization of natural resources, it is essential to focus the processes of environmental recovery from the point of view of the circular economy. In this context, it is important to highlight that lignocellulosic matter (as it is the case of phytoremediation biomass) can be used as the feedstock for the generation of carbonaceous materials that could be potentially used as adsorbents [7, 8], catalysts [9, 10], water treatment [11] or different electrochemical applications, including sensors or supercapacitors [12], avoiding the problem of treatment and disposal of these toxic wastes. In general, high-added value materials can be obtained by different processes of hydrothermal conversion of biomass in an oxygen-limited environment. Hydrochars

belong to these group of materials, and are produced through a process called hydrothermal carbonization (HTC), based on subjecting the biomass, mixed with water, to a temperature in the range from 180 to 240 ºC and pressure (from 2 to 6 MPa) [13]. By modifying the synthesis variables and applying subsequent surface modification processes, it is possible to improve the physical-chemical properties of the synthesized materials, such as surface area, hydrophobicity or electrical conductivity, thus being able to adapt the synthesis process to the application of interest [14, 15]. Specifically, a recent study has shown how it is possible to produce a material with properties similar to carbon black (CB) to be used as a cathode in a fuel cell from peanut waste treated with a HTC process and subsequent activation by pyrolysis [16]. Additional examples include the use of olives stones as catalysts supports for the wet peroxide oxidation to treat different persistent pollutants [17], or the usage of rice husks as adsorbent to remove hazardous heavy metal ions as Cu^{2+}, Fe^{3+} or Mn^{2+} [18]. Nevertheless, the promising results of these technologies mentioned competes with the possible use of these raw materials as human or animal food. Conversely, in the present work the raw material proposed is a toxic lignocellulosic waste that does not compete with any type of feeding, but it collaborates to avoid another environmental problem throughout the valorization of these materials.

Related to the value-added material expected, the electrochemical generation of H_2O_2 is an area of research whose importance has been growing in recent years, due to the wide range of applications of this reagent in environmental and industrial applications [19] and the expected compound annual growth rate (CAGR) index over 3% in the following five years [20]. Currently, almost all of the hydrogen peroxide consumed worldwide is produced by the anthraquinone process, which unfortunately has a high environmental impact [21]. A much more environmentally friendly alternative is the on-site electrochemical production of hydrogen peroxide. While this

can also be done anodically by water oxidation (Equation 1) [22, 23], the most common electrochemical pathway for producing hydrogen peroxide is based on the reduction of oxygen at the cathode of an electrochemical cell, according to the 2 electrons oxygen reduction reaction (2e-ORR), expressed by Equation 2 [24, 25].

$$2H_2O \rightarrow H_2O_2 + 2H^+ + 2e^- \quad [1]$$

$$O_2 + 2H^+ + 2e^- \rightarrow H_2O_2 \quad [2]$$

A big effort has been recently performed on improving the selectivity and activity of cathodes to improve the production of hydrogen peroxide by the 2e-ORR. One of the cathode materials that has been widely used in the promotion of this reaction consists of a conductive foam base material (titanium, aluminium or carbon) coated with a mixture of polytetrafluoroethylene (PTFE) and CB. The addition of PTFE is intended to control the hydrophobicity of the material related with the oxygen mass transfer ability [26], while the addition of CB increases the surface roughness and reduces ohmic losses, which are determining factors for the generation of triple phase contact points, which are essential for the efficient generation of hydrogen peroxide [27-31]. Many authors have evaluated alternatives to the use of CB-PTFE modified carbon substrates, as it is the case of the fabrication of oxidized carbon nanotubes [32], N-doped graphene [33], fluorine-doped porous carbons [34] or atomic-level tuning of carbon substrates [35], among others. Nonetheless, from the best of our knowledge, there is not previous works that aims to improve the sustainability of the hydrogen peroxide electrochemical synthesis by evaluating environmentally friendly alternatives to CB (conventionally obtained from petroleum residues) based on the basic principles of circular economy.

Based on this background, this work proposes the valorization of ~~plant~~ lignocellulosic biomass that does not compete with feeding of human or animals which is contaminated with heavy metals and comes from phytoremediation processes of mining waste, as feedstock for the synthesis of a carbon electrocatalytic material (CEM) that can be used as an alternative to CB for the production of hydrogen peroxide. The conversion of the polluted feedstock is performed through the application of an HTC stage and a subsequent activation process to improve properties these raw materials. These CEMs would be supported on Toray Paper®, that is a carbon fibre paper with excellent features such as high conductivity, high gas permeability, corrosion resistance. The viability of using this toxic waste as the starting material for the electrochemical production of hydrogen peroxide as well as the influence of the activation process on the improvement of physicochemical and electrochemical properties of the CEM were studied.

2. Materials and methods

2.1. Reagents

Titanium (IV) oxysulfate, polytetrafluoroethylene (PTFE) 60 % wt dispersion in H_2O, salicylic acid, 2,3-dihydroxybenzoic acid (2,3-dHBA) (HPLC grade), citric acid anhydrous, poly(vinylidene fluoride) (PVDF) and 1-methyl-2-pyrrolidinone anhydrous were supplied by Sigma Aldrich. 2-propanol, acetone, acetonitrile anhydrous and methanol were purchased to Scharlau at HPLC grade. Potassium hydroxide pellets 85 %, phosphoric acid 85 % and acetic acid were provided by Panreac. Carbon black (CB) Vulcan XC-72 (Fuelcell store), hydrogen peroxide 50 % (Proquimia S.L.), sodium sulfate anhydrous (Labkem), and 2,5-dihydroxybenzoic acid (2,5-dHBA) at HPLC

grade (Tokyo Chemical Industry) were the rest of the reagents employed. Milli-Q water (18.2 MΩ·cm) was used for preparing all aqueous solutions.

2.2. Carbon materials

The raw biomass used for all experiments as raw material was *Spergularia rubra*. This wild plant was obtained from the abandoned *San Quintín* mine located in Ciudad Real (Spain) (38º49'15.9''N 4º16'29.3''W). It naturally and spontaneously grows in mine tailings and it is able to retain high concentrations of heavy metals coming from the polluted soil, acting as a natural phytoremediation process [36]. *Spergularia rubra* was cleaned with Milli-Q water until all physically adsorbed impurities were removed and then dried for 24 h at 80 ºC before being crushed [37]. The metal content of the raw biomass is included in Table 1.

Table 1. Surface composition of raw biomass used in the present work evaluated with HR-SEM in atomic percentage.

2.2.1. Hydrothermal carbonization process

After this initial cleaning for the accumulator raw biomass, the hydrothermal carbonization (HTC) process was carried out. Hydrochar was obtained following this steps: (I) 7 g of *Spergularia rubra* were mixed with 54 mL of Milli-Q water (130 g L^{-1} ratio) [38] and stirred at 150 rpm for 30 min to warrant a homogeneous mixture; (II) the mixture was placed in a 100 mL Parr stainless Steel reactor and heated at 200 ºC in the oven for 2 h; (III) the product obtained was added to 800 mL of Milli-Q water when the reactor cooled down to room temperature, and stirred for 30 min at 300 rpm; (IV) finally, the hydrochar-water mixture was separated by filtration and the solid was dried for 24 h at 80 ºC.

2.2.2. Activation process

The hydrochar obtained after HTC process was thermally activated at different temperatures: 300 (HC300), 500 (HC500) and 1000 ºC (HC1000) under N_2 gas flowing (150 mL min^{-1}) in a tube furnace supplied by *Forns Hobersal* (Spain). The heating rate was 2 ºC min^{-1} and the final temperature was maintained for 30 min, with dwelling steps of 30 min at 300, 500 and 750 ºC [39]. Chemical activation was performed by mixing the hydrochar with 50 % KOH (HC-KOH) or 85 % H_3PO_4 (HC- H_3PO_4) in a 1:5 w/w ratio and stirring on top of a hotplate at 85 ºC for 2 h. The slurry was dried for 24 h and subsequently activated at 600 ºC, under the same N_2 gas flowing, with the same heating rate and the same dwelling steps as explained for thermal activation. The chemically activated hydrochars, once cooled to room temperature, were rinsed several times with Milli-Q water to remove all residual reagent until the pH of the rinse water stabilized [40].

2.2.3. Electrode manufacturing process

Modification of carbon fibre paper (CP) (Toray, Japan) was made by ultrasonic immersion following the next steps: (I) Pre-treatment: 15 min of ultrasonic bath with acetone, followed by two ultrasonic baths with Milli-Q water of 15 min each one. Then, the electrode was dried for 24 h at 80 ºC; (II) Immersion: the CEM was prepared mixing 20 mL of 2-propanol, 1 mg mL^{-1} of activated hydrochar or CB and 50 mg mL^{-1} of PTFE. The homogeneity of the CEM was ensured with 30 min of ultrasonic bath. After that, the CP electrode was immersed in the CEM for another 30 min of ultrasound; (III) Post-treatment: dry the CP electrode for 24 h at 80º C and annealing at 280 ºC for 1 h once the CEM has been deposited [41-43].

2.3. Physical-chemical characterization

Gas adsorption isotherms of N_2 at -196 ºC were employed to evaluate the porosity of the carbon materials with NOVA Touch LX^2 equipment, from Quantachrome Instruments. The samples were outgassed under vacuum for 2 h at 120 ºC and overnight at 30 ºC for 15 h [39]. This process was used to obtain the specific surface area (S_{BET}) of carbon samples.

For the thermogravimetric analysis (TG and DTG) Q50 TGA model from TA Instruments was used. Stabilisation was carried out at 100 ºC for 20 minutes to remove all existing moisture. Then, TG curves were obtained from 100 ºC to 800 ºC with a heating rate of 10 ºC min^{-1} at inert atmosphere (constant flow rate of 100 mL min^{-1} of N_2) [44]. TG curves were obtained to analyse the loss in mass of the different carbon materials with temperature.

For elementary analysis (carbon, nitrogen, hydrogen and sulfur) a Flash Smart™ from ThermoFisher was used. Instantaneous combustion of the carbonaceous sample was carried out at 950 ºC in pure oxygen atmosphere to obtain ashes. The resulting gases were transported by means of a carrier gas (He) through a reduction furnace. The separation of the different elements took place in a chromatographic column with a subsequent pass through a thermal conductivity detector to obtain the proportional signal of each of its components. Oxygen was determined by mass balance considering the concentration of metals also measured in the biomass (Table S2).

High-resolution scanning electron microscopy (HR-SEM) complemented with energy dispersive X-ray spectroscopy (EDS) detector was conducted on a ZEISS GeminiSEM 500 microscope to obtain images from the surface of the carbon materials. To evaluate the possible leaching of metals throughout the production of hydrogen

peroxide, the concentration of Fe^{2+} and Zn^{2+} in the liquid samples after H_2O_2 production tests was characterized by Spectroquant® tests (Sigma Aldrich).

Electrical conductivity of activated and non-activated materials was measured by the four-point probe method attending to the ASTM standard method D4496-87. Pellets were prepared with 90 wt% carbon material, 10 wt% of PVDF as binder and some drops of 1-methyl-2-pyrrolidinone. The mixtures were compacted with the 7 mm Pellet Die Assembly P/N GS03950 under 2 tons pressure. Each pellet elaborated had a thickness of 0.1 mm and a diameter of 7 mm. An Everbeing SR-4 four probe stand was used for resistance measuring. Potential differences were recorded when a current between 1 and 10 mA was applied directly to the surface of the pellets via the four probes. Resistivity was calculated as shown in Equation 3:

$$\rho = \frac{V}{I}\frac{\pi}{ln2}t \qquad [3]$$

Where ρ is the resistivity (Ω·m), V is the potential drop (V), I is the current intensity (A) and t is the thickness of the pellets (m). The conductivity, σ (S m^{-1}), is calculated as the inverse of the resistivity (1/ρ) [39].

2.4. Electrochemical characterization

2.4.1. H_2O_2 generation

Electrochemical experiments were conducted in a potentiostat/galvanostat PGSTAT302N from Autolab. Cyclic voltammetries (CVs) were conducted between 0.2 and -1.2 V with a scan rate of 0.05 V s^{-1}, using an Ag/AgCl reference electrode (KCl 3 M). H_2O_2 generation tests were performed by chronoamperometry (CA) at a constant

voltage of -0.9 V during 2 h, in 100 mL of 0.05 M Na_2SO_4 solution, with an Autolab cell under 900 rpm stirring speed and 2.5 L min^{-1} of air flow rate fed by a diffuser. The anode used for all experiments was graphite with an area of 4 cm^2 while the area of the cathode was 9 cm^2 [45]. The H_2O_2 concentration was measured with the titanium (IV) oxysulfate method as it was reported elsewhere [46]. The H_2O_2 concentration could be obtained finally by measuring the absorbance in a Shimadzu spectrophotometer.

The current efficiency (CE) was determined as shown in Equation 4:

$$CE = \frac{nFV[H_2O_2]}{I \cdot t} \quad [4]$$

Where n is the number of electrons transferred in the reaction (2), F is the Faraday constant (96487 C mol^{-1}), V is the electrolyte volume (L), $[H_2O_2]$ is the hydrogen peroxide concentration (M), I is the current intensity (A) ant t the reaction time (s).

2.4.2. OH· radicals' measurement

OH· radicals were measured with High Performance Liquid Chromatography (HPLC) detector JASCO MD-2018 Plus with deuterium and tungsten lamp, equipped with an Intersil C8 column (4.6 x 150 mm, 5 μm) at 296 nm of wavelength. Mobile phase was a mixture of citric acid (0.03 M), acetic acid (0.3 M), acetonitrile (10 %) and methanol (10 %) with different flow rates: 1 mL min^{-1} from 0 to 6 min, 1.5 ml min^{-1} from 7 to 15 min and 1 ml min^{-1} from 16 to 30 min. The column temperature was 25 ºC.

For OH· radicals' determination, a solution of 500 mg L^{-1} of salicylic acid and Na_2SO_4 0.05 M was employed for CA. The trapping of hydroxyl radicals by salicylic acid producing 2,5-dHBA and 2,3-dHBA was used for quantitative determination [47].

3. Results and discussions

3.1. Physical and chemical characterization of hydrochars from a biomass precursor

In this paper, hydrothermal carbonization was selected as the main thermal treatment applied to biomass wastes derived of phytoremediation treatments in order to promote the valorization of this material. The main reason to select HTC to improve structural properties of carbon materials is related to its versatility to be used with wet samples avoiding a pre-drying requirement of wet biomass and its milder carbonization conditions, indicating the lower energy consumption of HTC compared with pyrolytic processes [48]. To start with, the thermochemical stability of these samples, which are mainly composed of cellulose, hemicellulose and lignin, was evaluated with the aim to select further treatments to improve the electrochemical behaviour of these materials. Figure 1 (A) compares the thermal characteristics of the raw biomass and hydrochar generated at 130 g sample L^{-1} of water and 200ºC, an average value frequently chosen for these treatments in the literature [49], meanwhile Figure 1 (B) shows the results of the activated samples according to the procedures explained in detail in section 2.2.2.

Figure 1. TG-DTG curves corresponding to (A) dry raw biomass (solid line) and hydrochar (dotted line) and (B) Pyrolyzed hydrochars HC300, HC500, HC1000 and chemically activated hydrochars HC- KOH, HC-H_3PO_4. Hydrochar treated at 200 ºC with 130 g Solid L^{-1} ratio.

As it can be observed in Figure 1 (A), derivative thermogravimetric (DTG) curves show three main weight losses corresponding to each decomposition phase in raw materials (apart from the loss at 100 ºC associated to volatile organic matter): 1) hemicellulose (the highest peak in the range from 220 to 315 ºC); 2) cellulose around 350ºC and 3) lignin at 400-500ºC [50, 51]. In the case of the hydrochar obtained from HTC, it can be seen how the degradation occurs at higher temperature than the raw biomass. This shift to higher temperature values is explained due to a modification in

the nature of compounds caused by dehydration and decarboxylation reactions that transform the biomass in a more stable and carbon-rich material [52].

This trend of obtaining more stable materials when submitting the samples to higher temperatures is confirmed by analyzing the results gathered in Figure 1 (B). In this line, two peaks related with the degradation of two different type of compounds can be seen at 300ºC, meanwhile just a big loss around 550 ºC was observed for the sample activated at 500ºC, and finally a very slight reduction of weight was determined with the hydrochar pyrolyzed at 1000ºC. Regarding to the chemically activated hydrochars, different behaviors with each type of precursors selected were found. The activation with a basic-pH reagent (KOH) showed two mass losses around 400ºC and 600ºC, which indicate that the carbon surface and the structure were different with the synthesis of potassium carbonate and potassium oxide that increase the porosity or modify the polarity of these carbon materials (as it would be discussed below). In the case of activated hydrochar with H_3PO_4, it seems that the behavior is similar than the HC1000 because lignin is degraded and a cross-link structure was formed that makes more stable the carbon materials. A more detailed explanation of the influence of H_3PO_4 will be given at the end of this section.

However, to classify and compare all carbon materials obtained and to estimate some properties connected with the further electrochemical applications required, van Krevelen diagram is shown (Figure 2) as it provides a helpful classification of carbon materials (typically applied to biomass, hydrocarbons and fossil fuels) in connection with their origin and compositional evolution (*i.e.* thermal history) according with their atomic H/C and O/C ratio. It was shown the evolution in the atomic H/C and O/C ratios with different pyrolytic and chemical treatments and compared with the value of CB, which is a petroleum derivate widely applied in electrochemical engineering to promote

the generation of hydrogen peroxide via the 2e-ORR, as previously stated in the introduction section.

Figure 2. Van Krevelen diagram for the hydrochars synthesized with pyrolytic treatments and chemical activations methods. Carbon black (black point) was added for comparison purposes. (A) Linear scale (B) Logarithmic scale.

It was observed how very similar properties were obtained in the analysis of hydrochars in terms of elemental analysis in comparison with raw biomass because of the mild thermal conditions used (200 ºC). However, there is a paramount influence in the activated materials because HTC reduces the ash accumulated in solids and keeps them mainly in the liquid products, increasing the effects of the following treatments [53]. Generally, lower H/C and O/C mean a higher coalification degree, although H/C is related with the aromaticity of the carbon atoms, whereas the O/C ratio displays the extent of surface functionalization. In this line, the reduction of H/C ratio in the pyrolyzed hydrochars is related to dehydration reactions but also decarboxylation because it was observed a decrease in the Carbon Yield (CY) (Table S1) obtained when temperature of pyrolysis increases. Additionally, in Table S1 was also shown the elemental composition of carbons including the presence of heavy metals (derived of the soil regeneration treatments) in raw and treated carbon materials. The presence of metals as zinc, iron or lead might have a relevant importance in the thermal treatments, reducing the temperature to promote a more ordered structure or improve other physicochemical properties as electric conductivity or porosity that would require more energy with conventional treatments (further explained in the following sections).

Regarding to chemical activated compounds, the adding of other precursors modify the intermolecular forces and enhances the condensation of organics but O/C

ratio is rather constant which means that they keep some functionalities. The decrease of H/C ratio is related with the lower aromaticity, the increasing of hydrophobic properties and the activation of gas transfer channels for the O_2.

Then, to evaluate how these changes can affect the surface availability for ORR and triple electrolyte/electrode/oxygen interfaces when these materials are casted on carbon paper (Toray®), it was evaluated the porosity with N_2 adsorption/desorption isotherms (Figure 3a). Another important feature to electrochemical applications is the electrical conductivity (Figure 3b) as an increased value of this parameter means a reduction of ohmic losses.

Figure 3. (A) Nitrogen adsorption-desorption isotherms and (B) electric conductivity of Biomass, HC, HC300, HC500, HC1000, HC-KOH, HC-H_3PO_4 and CB. Electrical conductivity of Toray paper was also added for comparison purposes; b.d.l = below detection limit.

Isotherms of HC500 and HC1000 are comparable and correspond to type II of IUPAC classification [54]. Below p/p0, the physisorption of N_2 fills the micropores first and then, at p/p0= 0.05-0.85, N_2 is adsorbed in larger pores. Above p/p0= 0.8, the adsorbed volumes further increase because of additional N_2 adsorption inside pores higher than 10 nm in diameter. In the case of HC300, the porosity is not developed and just a low volume of mesopores according with the slope of isotherm has been generated. These pyrolyzed samples were compared with the solid derived of HTC that do not show any porosity (4 m^2/g). Isotherms of HC-KOH and HC-H_3PO_4 correspond to the type IV of IUPAC classification according to the higher volume of N_2 adsorbed and the hysteresis loop observed which indicates a capillary condensation during the desorption. The type of hysteresis loop broadened significantly, spanning from 0.4 up to 0.9 of relative pressures which is typical of mesoporosity with a non-rigid pore

structure. Specific Surface areas from Brunauer-Emmett-Teller (BET) model are listed in Table S2, adding the volume of micropores (Wo) from the Dubinin Raduskevich equation that indicate the larger specific Surface area obtained for HC-KOH (1097 m^2 g^{-1}) followed by HC-H_3PO_4 (704 m^2 g^{-1}). Results confirm the positive effect of these compounds to generate more mesoporous structures that enhance gas channels [55].

Regarding electrical conductivity, it can be seen how this parameter is not totally related with the porosity because CB, a material with medium porosity (218 m^2 g^{-1}) [56], is the most conductive material and, on contrary, the electrical conductivity of HC1000 (with 283 m^2 g^{-1} of surface area) and chemically activated hydrochars is lower than CB. These results can be associated to the graphitic structure and the number of defects presented in the samples as it was reported in other study with nitrogen-doped carbon network with cobalt species [57]. Thus, to clarify about the morphology of these materials some HR-SEM images about the microscopic surface details and microstructures of pyrolyzed hydrochars, HC-KOH and HC-H_3PO_4 (Figure 4) were evaluated.

Figure 4. HR-SEM images of the changes in the structure of treated biomass samples. (A) HC, (B) HC300, (C) HC500, (D) HC1000, (E) HC-KOH, (F) HC-H_3PO_4

Lignocellulosic structures slightly degraded can be seen in the biomass after HTC due to the soft conditions in terms of temperature and pressure that do not promote higher changes in the elemental composition neither in the original structure of the biomass. Nevertheless, this previous stage is very important because it can remove the content of volatile matter initially presented in the feedstock that could negatively affect the development of micro and mesoporosity after the washing of the solid product

obtained [58]. Figures 4 B, C and D show the development of microspheres on the surface, related to the dehydration of polymers. It can be seen how the structure morphology is modified and the specific surface area increased despite the low intensity of this effect in the HC300 because it is only related with the degradation of hemicellulose, in HC500 is related with the degradation of both hemicellulose and cellulose and in the last pyrolyzed sample (HC1000) the lignin is also degraded in the structure. The increase of temperature seems to accelerate the process of formation of nanospheres and microfiber fragmentation due to the destruction of the original structure. Figures 4 E,F related to the HC-KOH and HC-H_3PO_4 reveal a more wrinkled morphology compared with the pyrolyzed hydrochars and an interconnected porous network structure which is in agreement with the higher BET surface area determined with the N_2 adsorption/desorption isotherms presented in the Table S2. These structures are promoted by the different activation mechanisms [59]. The catalytic effect of H_3PO_4 contributes to bond cleavage reactions, which promote the decomposition of hydrochar and the corrosive nature of H_3PO_4 enhances the hydrolysis of lignocellulose compounds. In the case of KOH, the lower ash content and their interaction of potassium with carbon lead to the formation of mesopores and the cross-link structure shown in the SEM images [60]. Such unique morphological features seem to be beneficial for the diffusion of oxygen molecules in $2e^-$ ORR [61-63].

Next, to determine the real influence of these physicochemical properties in the $2e^-$ ORR proposed, cyclic voltammetries (CV) were assessed to determine the electric intensity in each case when a constant voltage was applied.

3.2. Electrochemical characterization of hydrochars to generate hydrogen peroxide

CV was chosen as a short test to determine the efficiency of electron transfer processes and thus, to evaluate their catalytic properties for the $2e^-$ ORR. The potential sweep of the working electrode (cathode) was controlled *vs* Ag/AgCl, and potential selected was between 0.2 and -1.2 V *vs* Ag/AgCl. A more negative potential could lead to water hydrolysis [64]. The counter electrode (anode) was a cylindrical bar of graphite (4 cm^2 of external area). Experiments with bare CP, CP with PTFE and CP with CB/PTFE deposited were carried out to compare the electrocatalytic activity of both with those of the carbonaceous materials tested. The electric currents measured in the working electrode during the potential scans for all materials are registered in Figure 5.

Figure 5. Cyclic voltammetries for bare CP and CP with deposited CB compared with: (A) HC300, HC500 and HC1000 and (B) HC-KOH and HC-H_3PO_4. Reference electrode used: Ag/AgCl (KCl 3 M). Anode: Graphite. Electrolyte: 100 mL of 0.05 M Na_2SO_4 solution. Stirring rate: 900 rpm. Constant air flow: 2.5 L min^{-1}. Scan rate: 50 mV s^{-1}. Two cycles were performed for each material.

As can be seen in Figures 5 (A) and (B), any current landing was observed in samples tested, which means that there is no limiting mass transfer of O_2 at the cathode surface at these potentials [65]. The (negative) increase of the electric current under a constant oxygen flow is mostly related to $2e^-$ ORR (Eq. 2). However, the H_2 evolution reaction (Equation 5) and the O_2 reduction to H_2O (Equation 6) can also take place at the cathode, being more common at more negative potentials (-1.23 V *vs* SHE) [66, 67].

$$H_2O + 1e^- \rightarrow \frac{1}{2} H_{2\,(g)} + HO^- \quad [5]$$

$$O_{2\,(g)} + 2H_2O + 4e^- \rightarrow 4HO^- \quad [6]$$

The bare CP electrode achieved a maximum current of -22 mA (for all materials, all maximum currents were recorded at -1.2 V) and an increase in current at -0.8 V (onset potential), while the PTFE deposited on CP obtained the worst result (around 5

mA at -1,2V) because it seems that the few sites to generate H_2O_2 in the bare CP are blocked with PTFE. On contrary, electrode with deposited CB reached -58 mA and presented an onset potential of -0.6 V. This increase in intensity is not only due to an increase in the number of active sites, but also to an increase in the number of electrons exchanged [68, 69]. These active sites are related with the microporous and mesoporous structure generated in treated carbons and with surfaee properties as electrical conductivity because it enhances the oxygen reactivy and the availability of channels to increase the mass transference of reagents and products. According to this, it is important to fix the potential of $2e^-$ ORR avoiding the pathway of $4e^-$ORR that would give water as main product. Therefore, the HC-KOH electrode had a higher electrocatalytic activity due to the good properties of the deposited material and could presumably generate higher amounts of H_2O_2. Figure 5 (A) shows, on the one hand, how HC300 and HC500 did not improve the electrocatalytic activity of the bare CP. The onset potential ocurrs approximately at the same value (-0.8 V *vs* Ag/AgCl), but the maximum intensities reached remained below the CP reference material (- 8.5 mA for HC-500 and -16.7 mA for HC-300).

On the other hand, HC1000 did show a noticeable improvement. The onset potential is around -0.4 V vs Ag/AglCl and the maximum intensity was reached at -39.2 mA. Therefore, higher conductivity and active sites were promoted in HC1000 due to the destruction of many lignocellulosic structures derived of thermochemical treatment which have a paramount influence in the electrocatalytic power observed, considerably close to commercial CB. Moreover, Figure 5 (B) shows that the two chemical activations have a different electrocatalytic behaviour and just the HC-KOH shows even greater electrocatalytic activity than CB, although both (HC-H_3PO_4 and HC-KOH) have the highest specific surface area measured (Table S2). In the case of HC-H_3PO_4,

electrical intensity obtained during CV was lower than bare CP and just -7.18 mA was reached as the maximum value. On the contrary, HC-KOH obtained outstanding results, even improving the electrocatalytic values of CB. The onset potential appears even before than CB (at -0.2 V *vs* Ag/AgCl) and it reached a maximum value of -62.28 mA, which confirms that this carbon material has the best electrocatalytic performance and the relevant influence of carbonaceous materials for the electrocatalytic improvement of these electrodes.

Next, potentiostatic H_2O_2 electrogeneration tests of 120 minutes were performed at -0.9V *vs* Ag/AgCl. In this line, Figures 6 (A and B) show the H_2O_2 accumulation and current efficiency, CE (C and D), with cathodes modified with different CEMs.

Figure 6. Electrogeneration of H_2O_2 for: (A) HC300, HC500 and HC1000 and (B) HC-KOH and HC-H_3PO_4, and current efficiencies for HC300, HC500 and HC1000 (C) and HC-KOH and HC-H_3PO_4 (D), compared with bare CP and CP with deposited CB. E= -0.9 V, reference electrode used: Ag/AgCl (KCl 3 M). Anode: Graphite. Electrolyte: 100 mL of 0.05 M Na_2SO_4 solution. Stirring rate: 900 rpm. Constant air flow: 2.5 L min^{-1}.

Figure 6 (A) shows that all thermal activations improved H_2O_2 generation compared to bare CP (16.39 mg L^{-1}). However, all samples were far from the results obtained by commercial CB (156.24 mg L^{-1}). HC300 (23.33 mg L^{-1}) and HC500 (20.75 mg L^{-1}) obtained the lowest values, enhancing H_2O_2 production *vs* bare CP 42.34% and 26.60 % respectively. HC1000 achieved the best results with this thermal activation (42.18 mg L^{-1}), increasing 2.6 times the concentration obtained with bare CP and obtaining a 27 % of the concentration reached with commercial CB, which is a remarkable performance. Regarding the generation of H_2O_2 by chemically activated hydrochars (Figure 6.B), HC-H_3PO_4 showed a H_2O_2 production below the bare CP

(13.42 mg L^{-1}), despite its large surface area, as it was expected from the results previously commented on CV. On the contrary, HC-KOH achieved the highest H_2O_2 generation results of all activated hydrochars with 107.64 mg L^{-1}, which represented an outstanding 68.9 % of the CB generation.

At this point, it is worth noting that both HC-500 and HC-H_3PO_4 did not show the expected H_2O_2 production according to their specific surface area obtained (Table S2), which demonstrates that not only the presence of gas transfer channels for O_2 or the catalytic points are important to enhance the $2e^-$ORR to produce H_2O_2. Other properties as electrical conductivity, structural defects, stability of catalytic mixtures or chemical composition would have a relevant influence in the stability of the electrodes and hence in the subsequent generation of H_2O_2. For the specific case of the differences between KOH and H_3PO_4, they can be related to the capacity of potassium to enhance the reduction of O_2 acting as electrochemical promoter as it was previously reported in literature for other electrochemical reactions [70].

Other important results related to the H_2O_2 production tests are the confirmation of negligible leaching of metallic compounds contained in the cathodic electrodes through the carbon ink deposited on their surface. After different thermal/chemical treatments these compounds were integrated in the carbon structure and concentrations lower than 0.5 mg L^{-1} of each ion tested were detected in the liquid effluent after a whole experiment of H_2O_2 production.

Figures 6 (C) and (D) show current efficiencies calculated with Eq. 4. The decrease in CE observed in all test, even for commercial CB, can be explained due to the number of side reactions that may occur in parallel as a single-compartment cell was used. Reduction at the cathode (1.776 V *vs* SHE) (Equation 7), oxidation in the anode

(1.2 V *vs* SHE) (Equation 8) and self-decomposition (Equations 9, 10a, 10b) are some of the reactions that could decrease the efficiency of H_2O_2 synthesis [71-74]:

$$H_2O_2 + 2e^- + 2H^+ \rightarrow 2\ H_2O \quad [7]$$

$$H_2O_2 \rightarrow O_2 + 2H^+ + 2\ e^- \quad [8]$$

$$H_2O_2 \rightarrow H_2O + ½\ O_2 \quad [9]$$

$$H_2O_2 \leftrightarrow HO_2^- + H^+ \quad [10a]$$

$$H_2O_2 + HO_2^- \rightarrow O_2 + 2H^+ + 2e^- \quad [10b]$$

As it can be observed, materials with a lower electrocatalytic activity do not necessarily present lower values of current efficiency. In this line, although the electric current (for -0.9 V vs Ag/AgCl) of HC-500 is -2.9 mA the CE is around 60% and in the case of HC-300, the electric current is -5.7 mA but the CE is around 40% (20.9 mg L^{-1} of H_2O_2) because the theoretical value of H_2O_2 expected in this case is higher (54.5 mg L^{-1}) according with the total energy consumed. In this line, HC-KOH and HC-1000 achieved lower CEs (around 30%) which are similar than bare CP. This means that side reactions (Eqs 7-10) are more important in HC-KOH despite the higher generation of H_2O_2 than for HC-500 or HC-H_3PO_4, which are not good electrocatalytic materials for any electrochemical reaction taking place in the system.

Additionally, energy requirements were also shown (figures 6 e and f). As it can be observed, specific power consumption increases for higher concentrations accumulated of hydrogen peroxide, due to the reduction of current efficiency because of parasitic reactions (as previously explained). According to the results, it can be stated

that the power consumption registered (from 1 to 6 kWh kg^{-1} H_2O_2, depending on the final concentration of hydrogen peroxide) is in line with those presented by Perez-Serrano et al. [41], Ma PengFei et al. [45] and F.L. Silva et al. [75] all using undivided cells and carbon felt modified with PTFE/CB as cathode.

Apart from the parasitic reactions already mentioned (equations 7 to 10b), it is worth remembering an additional reaction that may be occurring in the system, due to the high metallic content of the plants (Table S1) used as feedstock. These metals may promote the well-known Fenton reaction, shown in equation 11 [71], which is usually carried out with Fe^{2+} but that can be also promoted by other heavy metals as Cu or Co [76-78]. Thus, to shed light on the promotion of this Fenton reaction by the materials tested in the present work, the production of hydroxyl radicals (E^o = + 2.80 *vs* SHE) was measured by following the hydroxylated derivatives of salicylic acid, as described in the experimental section [47]. Results are gathered in Figure 7.

$$H_2O_2 + Fe^{2+} \rightarrow \cdot OH + Fe^{3+} + OH^- \quad [11]$$

Figure 7. Hydroxyl radicals generation for: (A) HC300, HC500 and HC1000 and (B) HC-KOH and HC-H_3PO_4, compared with naked CP and CP with PTFE/CB deposited. E= -0.9 V, reference electrode used: Ag/AgCl (KCl 3 M). Anode: Graphite. Electrolyte: 100 mL of 0.05 M Na_2SO_4 and 500 mg L^{-1} of salicylic acid. Stirring rate: 900 rpm. Constant air flow: 2.5 L min^{-1}.

As it can be observed in Figure 7 (A) and (B), except for HC-H_3PO_4, all carbonaceous materials generated a higher amount of hydroxyl radicals than CB (0.174 mM). HC-1000 achieved the highest hydroxyl radical generation value (0.2552 mM) followed by HC-KOH (0.2419 mM), increasing the amount obtained with CB by 47 % and 40 % respectively. These results confirms that, as previously commented, the metal

composition of carbonaceous catalysts had a great influence in the conversion of H_2O_2 into hydroxyl radicals and promoted the Fenton process. The evolution of hydroxyl radical generation were slightly lower for HC300 and HC500, but still superior to the CB generation, with 0.1944 and 0.2086 mM respectively. These results agreed with those obtained in H_2O_2 generation: HC-KOH and HC-1000 activations had the greatest generation and HC300, HC500 and HC-H_3PO_4 had the lowest, which again supported the higher electrocatalytic capacity of the first two activated hydrochars compared to the last three ones.

The potential use of these materials for an enhanced electrochemical production of hydroxyl radicals is a paramount finding of the present work and allows this process not only to valorize these wastes as a potential alternative to CB but also to design upgraded electrochemical advanced oxidation processes. Due to the potential application of this enhanced production of hydroxyl radicals, these results will be further studied in future works.

4. Conclusions

Biomass wastes derived from a natural phytoremediation process was valorized in the present work by applying hydrothermal carbonization. After this first step, five activation processes were carried out, three pyrolysis (HC300, HC500 and HC1000) and two chemical modifications (HC-KOH and HC-H_3PO_4) to improve their physicochemical properties. Bare CP and CB-CP were employed as reference material to evaluate the performance. Physicochemical and electrochemical characterization were performed for each material. Results obtained showed that HC-KOH had the best

H_2O_2 generation performance achieving a 70 % of the CB production and the best structural properties. Additionally, some other conclusions have been drawn:

- HTC is an efficient pre-treatment alternative to improve the thermal resistance of obtained carbon materials that can substitute CB in CP electrodes to produce H_2O_2.
- Thermal and chemical post treatments of hydrochars reduce the H/C and O/C ratio and improve the porosity and electrical conductivity of these carbon materials.
- Regarding hydrogen peroxide production of pyrolyzed hydrochars, the best electrochemical behavior was observed with the highest treatment temperature (1000ºC) (42.18 mg L^{-1} of H_2O_2 was generated) that intensively degrades the materials, increasing electrical conductivity and porosity. However, basic treatment of hydrochar HC-KOH showed the best generation of hydrogen peroxide (107.64 mg L^{-1}), much higher than the acidic treatment HC-H_3PO_4 (27.14 mg L^{-1}).
- The electrocatalytic performance of HC-KOH clearly overcomes that of HC-H_3PO_4, although both materials present similar porosity and electrical conductivity, demonstrating that the electrocatalytic properties are not always in line with the physicochemical behaviour of the materials.
- Electrodes modified with HC-KOH and HC1000 materials generated higher concentration of OH· than CB, which indicates that although the accumulation of H_2O_2 is lower, side reactions involved in the production of a more powerful oxidant as OH· are enhanced.

Acknowledgements

Authors gratefully acknowledge the financial support of the *Junta de Comunidades de Castilla-La Mancha* and European Union through the European Regional Development Fund (project SBPLY/21/180501/000058) and *Diputación de Albacete* for the funding through the project DIPUAB-2022 MUÑOZMORALES. Furthermore, this work is part of the project TED2021-131810A-I00, funded by MCIN/AEI/10.13039/501100011033 and by the European Union "NextGenerationEU"/PRTR.

Conflict of interests

The authors confirm that this article content has no conflict of interest and declare that all authors have participated in the elaboration of the manuscript.

References

[1] C. Hadjipanagiotou, A. Christou, A.M. Zissimos, E. Chatzitheodoridis, S.P. Varnavas, Contamination of stream waters, sediments, and agricultural soil in the surroundings of an abandoned copper mine by potentially toxic elements and associated environmental and potential human health–derived risks: a case study from Agrokipia, Cyprus, Environmental Science and Pollution Research, 27 (2020) 41279-41298.
[2] U.O. Chukwura, A.S. Hursthouse, Evaluating controls on potentially toxic element release in circum-neutral mine water: a case study from the abandoned Pb–Zn mines of Leadhills and Wanlockhead, South of Scotland, United Kingdom, Environmental Earth Sciences, 79 (2020).
[3] M.B. Kurade, Y.-H. Ha, J.-Q. Xiong, S.P. Govindwar, M. Jang, B.-H. Jeon, Phytoremediation as a green biotechnology tool for emerging environmental pollution: A step forward towards sustainable rehabilitation of the environment, Chemical Engineering Journal, 415 (2021) 129040.
[4] G. Yu, H. Ullah, X. Wang, J. Liu, B. Chen, P. Jiang, H. Lin, G.I. Sunahara, S. You, X. Zhang, A. Shahab, Integrated transcriptome and metabolome analysis reveals the mechanism of tolerance to manganese and cadmium toxicity in the Mn/Cd hyperaccumulator Celosia argentea Linn, Journal of Hazardous Materials, 443 (2023).
[5] X. Wang, S. Luo, Y. Chen, R. Zhang, L. Lei, K. Lin, C. Qiu, H. Xu, Potential of Miscanthus floridulus associated with endophytic bacterium Bacillus cereus BL4 to remediate cadmium contaminated soil, Science of the Total Environment, 857 (2023).

[6] L. Rodríguez, B. González-Corrochano, H.L. Medina-Díaz, F.J. López-Bellido, F.J. Fernández-Morales, J. Alonso-Azcárate, Does environmental risk really change in abandoned mining areas in the medium term when no control measures are taken?, Chemosphere, 291 (2022).
[7] A. Fernandez-Sanroman, V. Acevedo-García, M. Pazos, M.A. Sanromán, E. Rosales, Removal of sulfamethoxazole and methylparaben using hydrocolloid and fiber industry wastes: Comparison with biochar and laccase-biocomposite, Journal of Cleaner Production, 271 (2020).
[8] L. Wang, Y. Wang, F. Ma, V. Tankpa, S. Bai, X. Guo, X. Wang, Mechanisms and reutilization of modified biochar used for removal of heavy metals from wastewater: A review, Science of the Total Environment, 668 (2019) 1298-1309.
[9] G.R. Surup, J.J. Leahy, M.T. Timko, A. Trubetskaya, Hydrothermal carbonization of olive wastes to produce renewable, binder-free pellets for use as metallurgical reducing agents, Renewable Energy, 155 (2020) 347-357.
[10] M. Gholizadeh, X. Hu, Q. Liu, Progress of using biochar as a catalyst in thermal conversion of biomass, Reviews in Chemical Engineering, 37 (2021) 229-258.
[11] J. Liu, J. Jiang, Y. Meng, A. Aihemaiti, Y. Xu, H. Xiang, Y. Gao, X. Chen, Preparation, environmental application and prospect of biochar-supported metal nanoparticles: A review, Journal of Hazardous Materials, 388 (2020).
[12] X. Cao, Z. Li, H. Chen, C. Zhang, Y. Zhang, C. Gu, X. Xu, Q. Li, Synthesis of biomass porous carbon materials from bean sprouts for hydrogen evolution reaction electrocatalysis and supercapacitor electrode, International Journal of Hydrogen Energy, 46 (2021) 18887-18897.
[13] M.H. Marzbali, S. Kundu, P. Halder, S. Patel, I.G. Hakeem, J. Paz-Ferreiro, S. Madapusi, A. Surapaneni, K. Shah, Wet organic waste treatment via hydrothermal processing: A critical review, Chemosphere, 279 (2021) 130557.
[14] Q. Wang, R. Guo, Z. Wang, D. Shen, R. Yu, K. Luo, C. Wu, S. Gu, Progress in carbon-based electrocatalyst derived from biomass for the hydrogen evolution reaction, Fuel, 293 (2021).
[15] H.S. Kambo, A. Dutta, A comparative review of biochar and hydrochar in terms of production, physico-chemical properties and applications, Renewable and Sustainable Energy Reviews, 45 (2015) 359-378.
[16] D. Schonvogel, M. Nowotny, T. Woriescheck, H. Multhaupt, P. Wagner, A. Dyck, C. Agert, M. Wark, Hydrothermal Carbonization-Derived Carbon from Waste Biomass as Renewable Pt Support for Fuel Cell Applications: Role of Carbon Activation, Energy Technology, 7 (2019) 1900344.
[17] B.M. Esteves, S. Morales-Torres, F.J. Maldonado-Hódar, L.M. Madeira, Sustainable iron-olive stone-based catalysts for Fenton-like olive mill wastewater treatment: Development and performance assessment in continuous fixed-bed reactor operation, Chemical Engineering Journal, 435 (2022) 134809-134809.
[18] N. Hossain, S. Nizamuddin, K. Shah, Thermal-chemical modified rice husk-based porous adsorbents for Cu (II), Pb (II), Zn (II), Mn (II) and Fe (III) adsorption, Journal of Water Process Engineering, 46 (2022) 102620.

[19] S. Li, J. Ma, F. Xu, L. Wei, D. He, Fundamental principles and environmental applications of electrochemical hydrogen peroxide production: A review, Chemical Engineering Journal, 452 (2023).
[20] HYDROGEN PEROXIDE MARKET - GROWTH, TRENDS, COVID-19 IMPACT, AND FORECASTS (2022 - 2027), Mordor Intelligence
[21] J.M. Campos-Martin, G. Blanco-Brieva, J.L.G. Fierro, Hydrogen Peroxide Synthesis: An Outlook beyond the Anthraquinone Process, Angew. Chem. Int. Ed., 45 (2006) 6962-6984.
[22] V. Viswanathan, H.A. Hansen, J.K. Nørskov, Selective Electrochemical Generation of Hydrogen Peroxide from Water Oxidation, The Journal of Physical Chemistry Letters, 6 (2015) 4224-4228.
[23] Z. Chen, S. Geng, Y. Wang, Y. Wang, S. Song, Boosting 2 e- water oxidation reaction on WO3 by F modification and revealing the mechanism by probing interfacial water structure, Applied Catalysis B: Environmental, 317 (2022).
[24] J.F. Pérez, J. Llanos, C. Sáez, C. López, P. Cañizares, M.A. Rodrigo, The jet aerator as oxygen supplier for the electrochemical generation of H2O2, Electrochimica Acta, 246 (2017) 466-474.
[25] G. O.S. Santos, P.J. M. Cordeiro-Junior, I. Sánchez-Montes, R. S. Souto, M. S. Kronka, M. R.V. Lanza, Recent advances in H2O2 electrosynthesis based on the application of gas diffusion electrodes: Challenges and opportunities, Current Opinion in Electrochemistry, 36 (2022).
[26] J. An, N. Li, Q. Zhao, Y. Qiao, S. Wang, C. Liao, L. Zhou, T. Li, X. Wang, Y. Feng, Highly efficient electro-generation of H2O2 by adjusting liquid-gas-solid three phase interfaces of porous carbonaceous cathode during oxygen reduction reaction, Water Research, 164 (2019) 114933-114933.
[27] J.F. Pérez, C. Sáez, J. Llanos, P. Cañizares, C. López, M.A. Rodrigo, Improving the Efficiency of Carbon Cloth for the Electrogeneration of H2O2: Role of Polytetrafluoroethylene and Carbon Black Loading, Industrial & Engineering Chemistry Research, 56 (2017) 12588-12595.
[28] N. Li, C. Huang, X. Wang, Y. Feng, J. An, Electrosynthesis of hydrogen peroxide via two-electron oxygen reduction reaction: A critical review focus on hydrophilicity/hydrophobicity of carbonaceous electrode, Chemical Engineering Journal, 450 (2022).
[29] P.J.M. Cordeiro Junior, A.S. Martins, G.B.S. Pereira, F.V. Rocha, M.A.R. Rodrigo, M.R.d.V. Lanza, High-performance gas-diffusion electrodes for H2O2 electrosynthesis, Electrochimica Acta, 430 (2022) 141067.
[30] A. Casanova, A. Gomis-Berenguer, A. Canizares, P. Simon, D. Calzada, C.O. Ania, Carbon Black as Conductive Additive and Structural Director of Porous Carbon Gels, Materials, 13 (2020) 217.
[31] C.O. Okoye, I. Jones, M. Zhu, Z. Zhang, D. Zhang, Manufacturing of carbon black from spent tyre pyrolysis oil – A literature review, Journal of Cleaner Production, 279 (2021) 123336.
[32] Z. Lu, G. Chen, S. Siahrostami, Z. Chen, K. Liu, J. Xie, L. Liao, T. Wu, D. Lin, Y. Liu, T.F. Jaramillo, J.K. Nørskov, Y. Cui, High-efficiency oxygen reduction to

hydrogen peroxide catalysed by oxidized carbon materials, Nature Catalysis, 1 (2018) 156-162.
[33] P. Su, M. Zhou, X. Lu, W. Yang, G. Ren, J. Cai, Electrochemical catalytic mechanism of N-doped graphene for enhanced H2O2 yield and in-situ degradation of organic pollutant, Applied Catalysis B: Environmental, 245 (2019) 583-595.
[34] K. Zhao, Y. Su, X. Quan, Y. Liu, S. Chen, H. Yu, Enhanced H2O2 production by selective electrochemical reduction of O2 on fluorine-doped hierarchically porous carbon, Journal of Catalysis, 357 (2018) 118-126.
[35] E. Jung, H. Shin, B.-H. Lee, V. Efremov, S. Lee, H.S. Lee, J. Kim, W. Hooch Antink, S. Park, K.-S. Lee, S.-P. Cho, J.S. Yoo, Y.-E. Sung, T. Hyeon, Atomic-level tuning of Co–N–C catalyst for high-performance electrochemical H2O2 production, Nature Materials, 19 (2020) 436-442.
[36] P. Campos, A.Z. Miller, S.A. Prats, H. Knicker, N. Hagemann, J.M. De la Rosa, Biochar amendment increases bacterial diversity and vegetation cover in trace element-polluted soils: A long-term field experiment, Soil Biology and Biochemistry, 150 (2020).
[37] A.H.A. Khan, A. Kiyani, M. Santiago-Herrera, J. Ibáñez, S. Yousaf, M. Iqbal, S. Martel-Martín, R. Barros, Sustainability of phytoremediation: Post-harvest stratagems and economic opportunities for the produced metals contaminated biomass, Journal of Environmental Management, 326 (2023) 116700.
[38] W. Tu, Y. Liu, Z. Xie, M. Chen, L. Ma, G. Du, M. Zhu, A novel activation-hydrochar via hydrothermal carbonization and KOH activation of sewage sludge and coconut shell for biomass wastes: Preparation, characterization and adsorption properties, J Colloid Interface Sci, 593 (2021) 390-407.
[39] A. Casanova, A. Gomis-Berenguer, A. Canizares, P. Simon, D. Calzada, C.O. Ania, Carbon Black as Conductive Additive and Structural Director of Porous Carbon Gels, Materials (Basel), 13 (2020).
[40] X. Zhang, B. Gao, J. Fang, W. Zou, L. Dong, C. Cao, J. Zhang, Y. Li, H. Wang, Chemically activated hydrochar as an effective adsorbent for volatile organic compounds (VOCs), Chemosphere, 218 (2019) 680-686.
[41] J.F. Pérez, A. Galia, M.A. Rodrigo, J. Llanos, S. Sabatino, C. Sáez, B. Schiavo, O. Scialdone, Effect of pressure on the electrochemical generation of hydrogen peroxide in undivided cells on carbon felt electrodes, Electrochim. Acta, 248 (2017) 169-177.
[42] F. Yu, M. Zhou, X. Yu, Cost-effective electro-Fenton using modified graphite felt that dramatically enhanced on H 2 O 2 electro-generation without external aeration, Electrochimica Acta, 163 (2015) 182-189.
[43] G. Ren, M. Zhou, M. Liu, L. Ma, H. Yang, A novel vertical-flow electro-Fenton reactor for organic wastewater treatment, Chemical Engineering Journal, 298 (2016) 55-67.
[44] J.S. Castro, P.P. Assemany, A.C.O. Carneiro, J. Ferreira, M.M. de Jesus Junior, F.A. Rodrigues, M.L. Calijuri, Hydrothermal carbonization of microalgae biomass produced in agro-industrial effluent: Products, characterization and applications, Sci Total Environ, 768 (2021) 144480.

[45] P. Ma, H. Ma, A. Galia, S. Sabatino, O. Scialdone, Reduction of oxygen to H2O2 at carbon felt cathode in undivided cells. Effect of the ratio between the anode and the cathode surfaces and of other operative parameters, Separation and Purification Technology, 208 (2019) 116-122.
[46] F. Yu, M. Zhou, X. Yu, Cost-effective electro-Fenton using modified graphite felt that dramatically enhanced on H2O2 electro-generation without external aeration, Electrochim. Acta, 163 (2015) 182-189.
[47] J.-F. Jen, M.-F. Leu, T.C. Yang, Determination of hydroxyl radicals in an advanced oxidation process with salicylic acid trapping and liquid chromatography, Journal of Chromatography A, 796 (1998) 283-288.
[48] A.A. Azzaz, B. Khiari, S. Jellali, C.M. Ghimbeu, M. Jeguirim, Hydrochars production, characterization and application for wastewater treatment: A review, Renewable and Sustainable Energy Reviews, 127 (2020) 109882-109882.
[49] A. Khosravi, H. Zheng, Q. Liu, M. Hashemi, Y. Tang, B. Xing, Production and characterization of hydrochars and their application in soil improvement and environmental remediation, Chemical Engineering Journal, 430 (2022) 133142.
[50] H. Yang, R. Yan, H. Chen, D.H. Lee, C. Zheng, Characteristics of hemicellulose, cellulose and lignin pyrolysis, Fuel, 86 (2007) 1781-1788.
[51] D. Díez, A. Urueña, R. Piñero, A. Barrio, T. Tamminen, Determination of Hemicellulose, Cellulose, and Lignin Content in Different Types of Biomasses by Thermogravimetric Analysis and Pseudocomponent Kinetic Model (TGA-PKM Method), Processes, 8 (2020).
[52] A. Raheem, Q. He, L. Ding, W. Dastyar, G. Yu, Evaluating performance of pyrolysis and gasification processes of agriculture residues-derived hydrochar: Effect of hydrothermal carbonization, Journal of Cleaner Production, 338 (2022) 130578-130578.
[53] Y. Zhang, Q. Jiang, W. Xie, Y. Wang, J. Kang, Effects of temperature, time and acidity of hydrothermal carbonization on the hydrochar properties and nitrogen recovery from corn stover, Biomass Bioenergy, 122 (2019) 175-182.
[54] K.S.W. Sing, 7 - Assessment of Surface Area by Gas Adsorption, in: F. Rouquerol, J. Rouquerol, K.S.W. Sing, P. Llewellyn, G. Maurin (Eds.) Adsorption by Powders and Porous Solids (Second Edition), Academic Press, Oxford, 2014, pp. 237-268.
[55] C. Li, C. Hu, Y. Song, Y.-M. Sun, W. Yang, M. Ma, Graphene-based synthetic fabric cathodes with specific active oxygen functional groups for efficient hydrogen peroxide generation and homogeneous electro-Fenton processes, Carbon, 186 (2022) 699-710.
[56] D. Schonvogel, J. Müller-Hülstede, P. Wagner, I. Kruusenberg, K. Tammeveski, A. Dyck, C. Agert, M. Wark, Stability of Pt Nanoparticles on Alternative Carbon Supports for Oxygen Reduction Reaction, Journal of The Electrochemical Society, 164 (2017) F995-F1004.
[57] S. Zhang, S. Li, J. Liu, L. Kan, F. Rong, L. He, Z. Zhang, Multiple active cobalt species embedded in microporous nitrogen-doped carbon network for the selective production of hydrogen peroxide, J. Colloid Interface Sci., 631 (2023) 101-113.
[58] N. Baccile, J. Weber, C. Falco, M. Titirici, Sustainable Carbon Materials from Hydrothermal Processes, 2013, pp. 151-211.

[59] S. Yorgun, D. Yıldız, Preparation and characterization of activated carbons from Paulownia wood by chemical activation with H3PO4, Journal of the Taiwan Institute of Chemical Engineers, 53 (2015) 122-131.
[60] U. Thubsuang, S. Laebang, N. Manmuanpom, S. Wongkasemjit, T. Chaisuwan, Tuning pore characteristics of porous carbon monoliths prepared from rubber wood waste treated with H3PO4 or NaOH and their potential as supercapacitor electrode materials, Journal of Materials Science, 52 (2017).
[61] T.-P. Fellinger, F. Hasché, P. Strasser, M. Antonietti, Mesoporous Nitrogen-Doped Carbon for the Electrocatalytic Synthesis of Hydrogen Peroxide, Journal of the American Chemical Society, 134 (2012) 4072-4075.
[62] K.M. Nair, V. Kumaravel, S.C. Pillai, Carbonaceous cathode materials for electro-Fenton technology: Mechanism, kinetics, recent advances, opportunities and challenges, Chemosphere, 269 (2021) 129325.
[63] K. Sheoran, V. Kumar Thakur, S. Singh Siwal, Synthesis and overview of carbon-based materials for high performance energy storage application: A review, Materials Today: Proceedings, (2021).
[64] L. Yu, J. Lin, M. Zheng, M. Chen, Y. Ding, Homogeneous electrocatalytic water oxidation at neutral pH by a robust trinuclear copper(ii)-substituted polyoxometalate, Chem Commun (Camb), 54 (2018) 354-357.
[65] H. Li, H. Liu, Z. Jong, W. Qu, D. Geng, X. Sun, H. Wang, Nitrogen-doped carbon nanotubes with high activity for oxygen reduction in alkaline media, International Journal of Hydrogen Energy, 36 (2011) 2258-2265.
[66] W.R.P. Barros, T. Ereno, A.C. Tavares, M.R.V. Lanza, In Situ Electrochemical Generation of Hydrogen Peroxide in Alkaline Aqueous Solution by using an Unmodified Gas Diffusion Electrode, ChemElectroChem, 2 (2015) 714-719.
[67] I. Moussallem, J. Jörissen, U. Kunz, S. Pinnow, T. Turek, Chlor-alkali electrolysis with oxygen depolarized cathodes: history, present status and future prospects, Journal of Applied Electrochemistry, 38 (2008) 1177-1194.
[68] M. Mazzucato, C. Durante, Insights on Oxygen Reduction Reaction to H2O2: The role of functional groups and textural properties on the activity and selectivity of doped carbon electrocatalysts, Current Opinion in Electrochemistry, 35 (2022).
[69] N. Daems, T. Breugelmans, I.F.J. Vankelecom, P.P. Pescarmona, Influence of the Composition and Preparation of the Rotating Disk Electrode on the Performance of Mesoporous Electrocatalysts in the Alkaline Oxygen Reduction Reaction, ChemElectroChem, 5 (2018) 119-128.
[70] A. de Lucas-Consuegra, F. Dorado, C. Jiménez-Borja, J.L. Valverde, Influence of the reaction conditions on the electrochemical promotion by potassium for the selective catalytic reduction of N2O by C3H6 on platinum, Applied Catalysis B: Environmental, 78 (2008) 222-231.
[71] E. Petrucci, A. Da Pozzo, L. Di Palma, On the ability to electrogenerate hydrogen peroxide and to regenerate ferrous ions of three selected carbon-based cathodes for electro-Fenton processes, Chemical Engineering Journal, 283 (2016) 750-758.
[72] M. Panizza, G. Cerisola, Electrochemical generation of H2O2 in low ionic strength media on gas diffusion cathode fed with air, Electrochimica Acta, 54 (2008) 876-878.

[73] W. Zhou, J. Gao, L. Rajic, Y. Ding, Y. Zhao, H. Zhao, X. Meng, Y. Wang, K. Kou, Y. Xu, S. Wu, Y. Qin, A.N. Alshawabkeh, Drastic Enhancement of H(2)O(2) Electro-generation by Pulsed Current for Ibuprofen Degradation: Strategy Based on Decoupling Study on H(2)O(2) Decomposition Pathways, Chem Eng J, 338 (2018) 709-718.
[74] A.D. Pozzo, L.D. Palma, C. Merli, E. Petrucci, An experimental comparison of a graphite electrode and a gas diffusion electrode for the cathodic production of hydrogen peroxide, Journal of Applied Electrochemistry, 35 (2005) 413-419.
[75] F.L. Silva, R.M. Reis, W.R.P. Barros, R.S. Rocha, M.R.V. Lanza, Electrogeneration of hydrogen peroxide in gas diffusion electrodes: Application of iron (II) phthalocyanine as a modifier of carbon black, Journal of Electroanalytical Chemistry, 722-723 (2014) 32-37.
[76] H. Kim, J. Lim, S. Lee, H.H. Kim, C. Lee, J. Lee, W. Choi, Spontaneous Generation of H(2)O(2) and Hydroxyl Radical through O(2) Reduction on Copper Phosphide under Ambient Aqueous Condition, Environ Sci Technol, 53 (2019) 2918-2925.
[77] X. Ma, Y. Cheng, Y. Ge, H. Wu, Q. Li, N. Gao, J. Deng, Ultrasound-enhanced nanosized zero-valent copper activation of hydrogen peroxide for the degradation of norfloxacin, Ultrason Sonochem, 40 (2018) 763-772.
[78] X.X. Guo, T.T. Hu, B. Meng, Y. Sun, Y.-F. Han, Catalytic degradation of anthraquinones-containing H2O2 production effluent over layered Co-Cu hydroxides: Defects facilitating hydroxyl radicals generation, Applied Catalysis B: Environmental, 260 (2020).

TABLES

Table 1. Surface composition of raw biomass used in the present work evaluated with HR-SEM in atomic percentage.

	C	O	Mg	Al	Si	P	S	K	Ca	Fe	Zn	Pb
Raw biomass	65.77	31.32	0.15	0.14	0.40	0.07	0.27	0.94	0.373	0.33	0.48	0.03

FIGURES

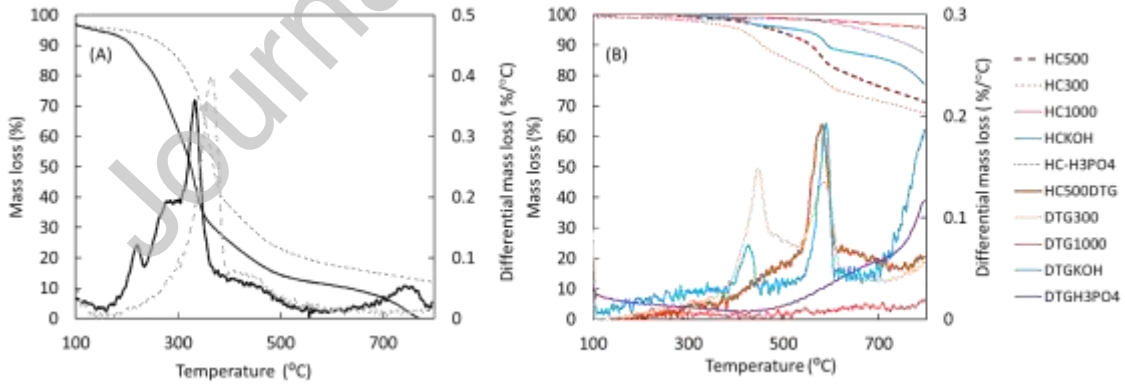

Figure 1. TG-DTG curves corresponding to (A) dry raw biomass (solid line) and hydrochar (dotted line) and (B) Pyrolyzed hydrochars HC300, HC500, HC1000 and chemically activated hydrochars HC- KOH, HC-H_3PO_4. Hydrochar treated at 200 ºC with 130 g Solid L^{-1} ratio.

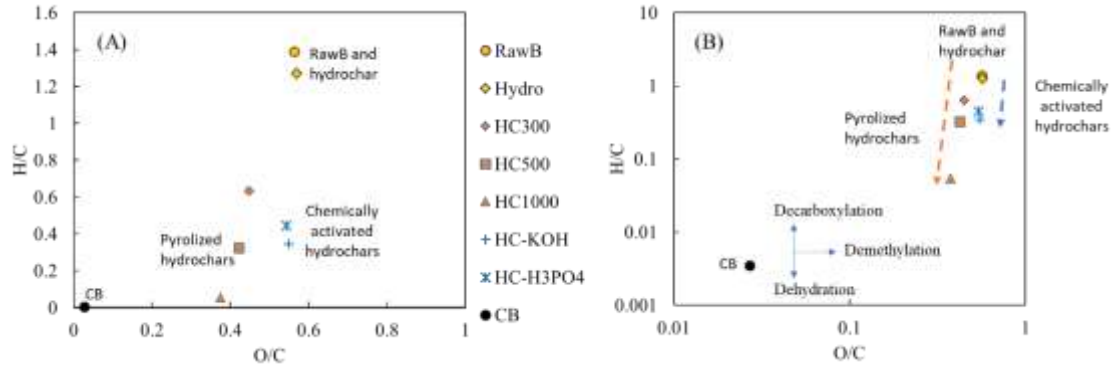

Figure 2. Van Krevelen diagram for the hydrochars synthesized with pyrolytic treatments and chemical activations methods. Carbon black (black point) was added for comparison purposes. (A) Linear scale (B) Logarithmic scale.

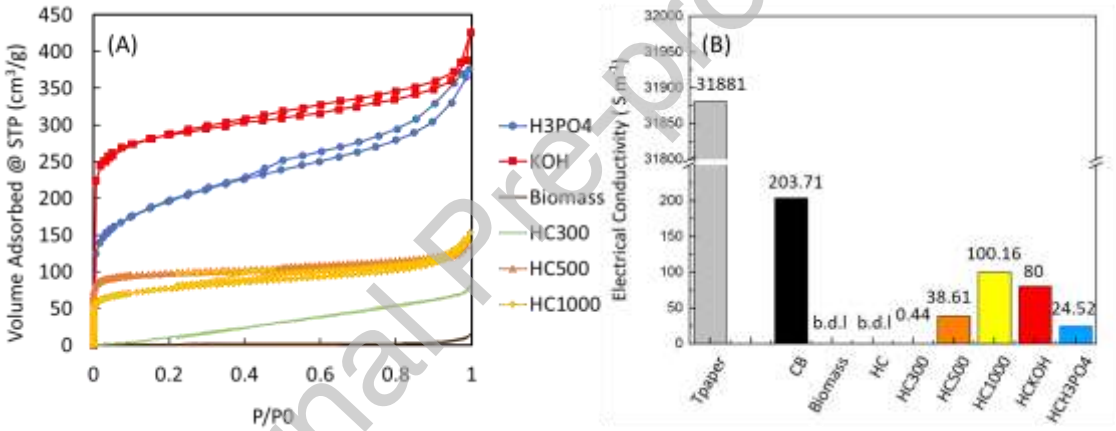

Figure 3. (A) Nitrogen adsorption-desorption isotherms and (B) electric conductivity of Biomass, HC, HC300, HC500, HC1000, HC-KOH, HC-H_3PO_4 and CB. Electrical conductivity of Toray paper was also added for comparison purposes; b.d.l = below detection limit.

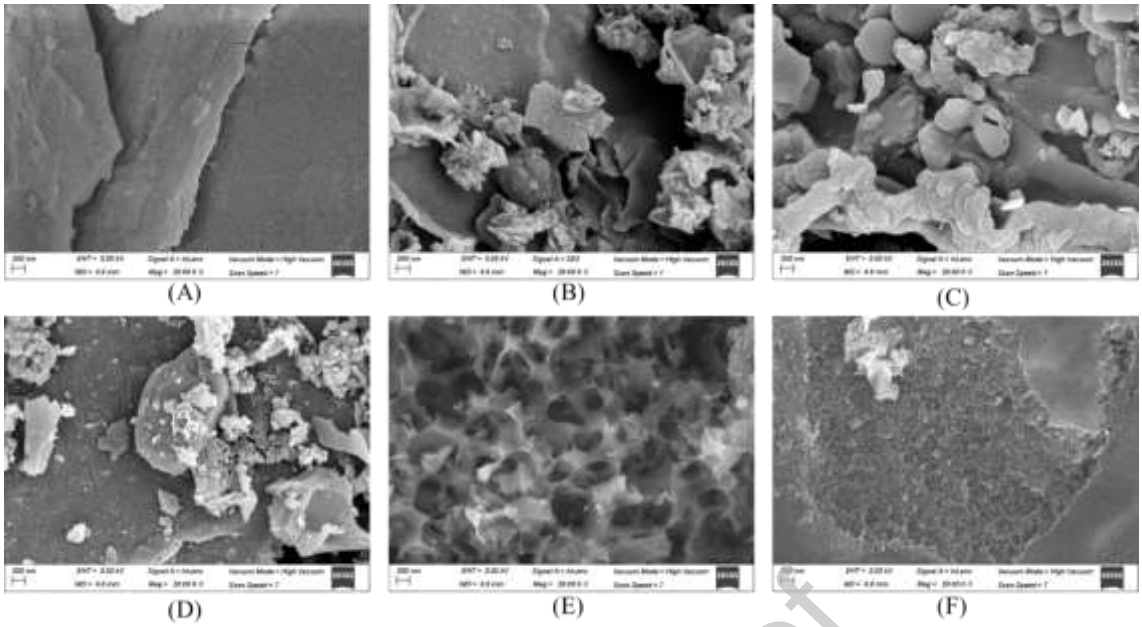

Figure 4. HR-SEM images of the changes in the structure of treated biomass samples. (A) HC, (B) HC300, (C) HC500, (D) HC1000, (E) HC-KOH, (F) HC-H_3PO_4

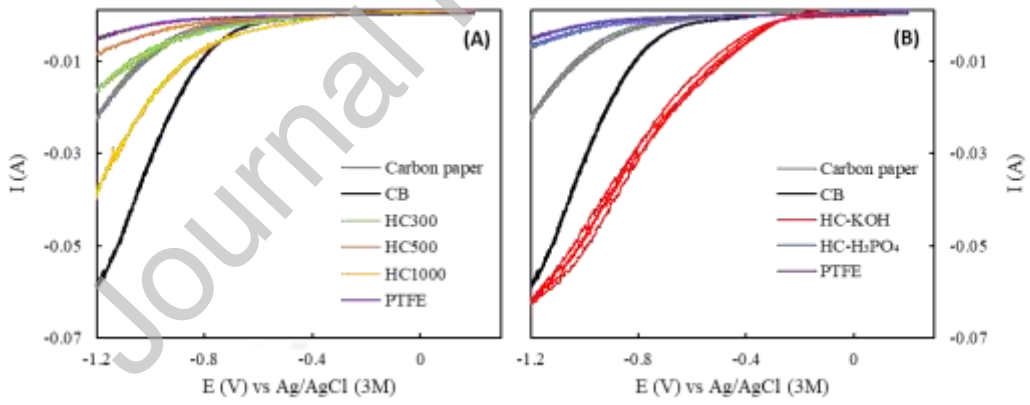

Figure 5. Cyclic voltammetries for bare CP, CP with PTFE and CP with CB deposited compared with: (A) HC300, HC500 and HC1000 and (B) HC-KOH and HC-H_3PO_4. Reference electrode used: Ag/AgCl (KCl 3 M). Anode: Graphite. Electrolyte: 100 mL of 0.05 M Na_2SO_4 solution. Stirring rate: 900 rpm. Constant air flow: 2.5 L min^{-1}. Scan rate: 50 mV s^{-1}. Two cycles were performed for each material.

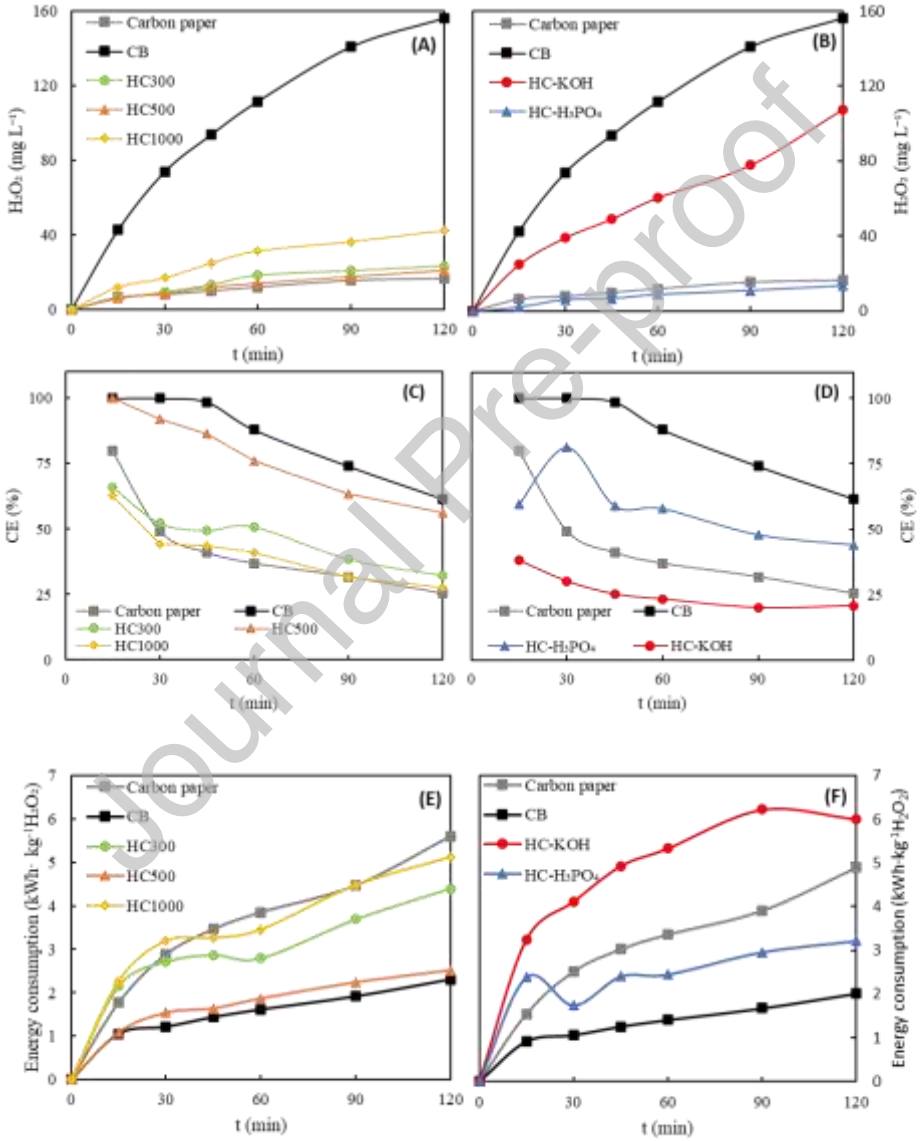

Figure 6. Electrogeneration of H_2O_2 for: (A) HC300, HC500 and HC1000; (B) HC-KOH and HC-H_3PO_4, and current efficiencies (CE) for HC300, HC500 and HC1000 (C) and HC-KOH and HC-H_3PO_4 (D), compared with bare CP and CP with deposited CB; Energy consumption (KWh) per kg of H_2O_2 for (E) HC300, HC500 and HC1000; (F) HC-KOH and HC-H_3PO_4 compared with bare CP and CP with deposited CB . ΔV= -0.9 V, reference electrode used:

Ag/AgCl (KCl 3 M). Anode: Graphite. Electrolyte: 100 mL of 0.05 M Na_2SO_4 solution. Stirring rate: 900 rpm. Constant air flow: 2.5 L min^{-1}.

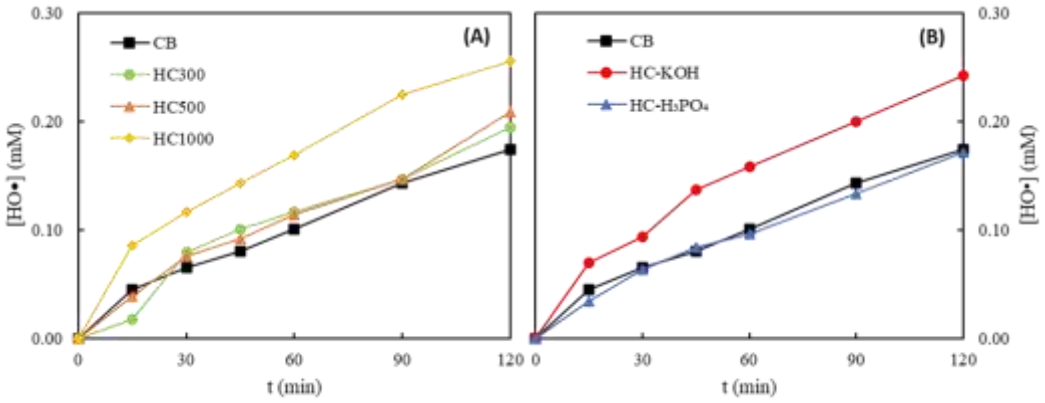

Figure 7. Hydroxyl radicals generation for: (A) HC300, HC500 and HC1000 and (B) HC-KOH and HC-H_3PO_4, compared with naked CP and CP with deposited CB. E= -0.9 V, reference electrode used: Ag/AgCl (KCl 3 M). Anode: Graphite. Electrolyte: 100 mL of 0.05 M Na_2SO_4 and 500 mg L^{-1} of salicylic acid. Stirring rate: 900 rpm. Constant air flow: 2.5 L min^{-1}.

Graphical abstract

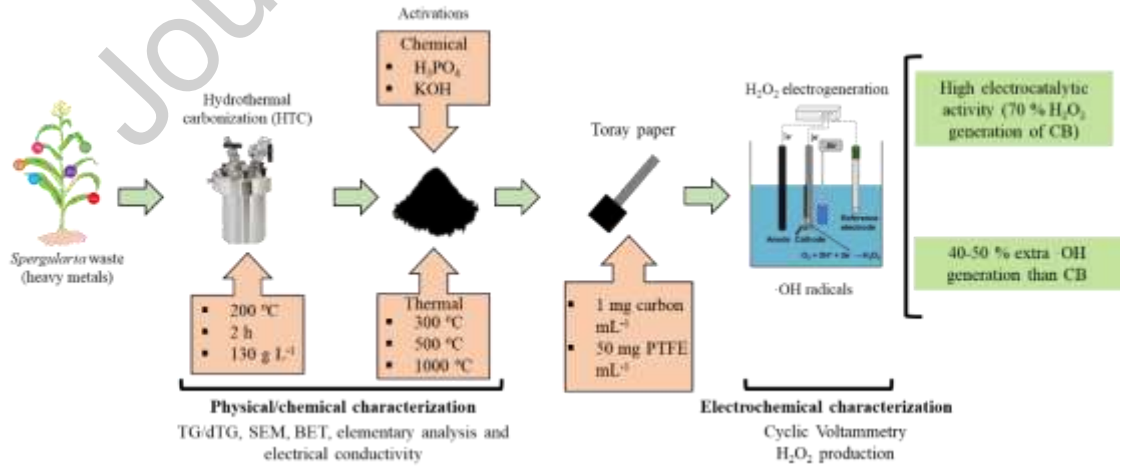

CRediT author statement

Álvaro Ramírez: Investigation, Visualization, Writing-Original Draft, Data Curation; Martín Muñoz-Morales: Writing - Review & Editing, Supervision, Funding acquisition; Francisco Jesús Fernández-Morales: Writing - Review & Editing, Supervision; Javier Llanos: Conceptualization, Methodology, Writing - Review & Editing, Funding acquisition, Project administration.

Declaration of interests

☒ The authors declare that they have no known competing financial interests or personal relationships that could have appeared to influence the work reported in this paper.

☐ The authors declare the following financial interests/personal relationships which may be considered as potential competing interests: